

Bioinspired Design Process for an Underwater Flying and Hovering Vehicle

AUTHORS

Jason D. Geder
 John S. Palmisano
 Ravi Ramamurti
 Marius Pruessner
 Banahalli Ratna
 Naval Research Laboratory

William C. Sandberg
 Science Applications
 International Corporation

Background

Biologists and zoologists have been studying fish swimming for many decades, and several comprehensive texts and papers exist (Breder, 1926; Lindsey, 1978; Alexander, 1983; Azuma, 1992; Blake, 1983; Webb, 1975, 1984; Videler, 1993; Sfakiotakis et al., 1999). The experimental studies of fish swimming bio-dynamics have become increasingly quantitative as measurement technology has improved. The use of high-speed photography shed light upon the details of fin deformation (Gibb et al., 1994; Walker & Westneat, 1997). Laser light scattering techniques enabled observations of not only the fish body and fin dynamics but also the velocity field about the fish and in the wake (Drucker & Lauder, 1999, 2002; Gharib et al., 2002; Bartol et al., 2003). Vehicle designers are able to draw upon such rich data sets as they embark upon designs. But where does one begin?

A bioinspired vehicle design should begin, according to Webb (2004), by specifying the performance goals of

ABSTRACT

We review here the results obtained during the past several years in a series of computational and experimental investigations aimed at understanding the origin of high-force production in the flapping wings of insects and the flapping and deforming fins of fish and the incorporation of that information into bioinspired vehicle designs. We summarize the results obtained on pectoral fin force production, flapping and deforming fin design, and the emulation of fish pectoral fin swimming in unmanned vehicles. In particular, we discuss the main results from the computational investigations of pectoral fin force production for a particular coral reef fish, the bird wrasse (*Gomphosus varius*), whose impressive underwater flight and hovering performance matches our vehicle mission requirements. We describe the tradeoffs made between performance and produceability during the bio-inspired design of an actively controlled curvature pectoral fin and the incorporation of it into two underwater flight vehicles: a two-fin swimming version and four-fin swimming version. We describe the unique computational approach taken throughout the fin and vehicle design process for relating fin deformation time-histories to specified desired vehicle dynamic behaviors. We describe the development of the vehicle controller, including hardware implementation, using actuation of the multiple deforming flapping fins as the only means of propulsion and control. Finally, we review the comparisons made to date between four-fin vehicle experimental trajectory measurements and controller simulation predictions and discuss the incorporation of those comparisons into the controller design.

Keywords: bio-inspired robotics, pectoral fin, unmanned systems, computational fluid dynamics

the desired mission first and then examining those living creatures whose performance is relevant. These creatures have evolved to meet all their needs, and the maneuvering enabled by these needs may intersect with the performance requirements driving a vehicle design. However, since the living creatures selected for study are most likely not optimized for the mobility characteristics that are driving the design, one should not copy nature but instead be guided by it. This point of caution to designers has been made many times by biologists (Combes & Daniel, 2001;

Wainwright et al., 2002; Collar et al., 2008).

The mission selected for the Naval Research Laboratory (NRL) swimming vehicle, which we describe below, requires precise low-speed maneuvering and excellent hovering in a complex near-shore environment in addition to excellent position-keeping in tidal currents. Cost and mechanical simplicity constraints demanded a rigid hull. This eliminated undulatory swimming fish as a primary means of design inspiration, and instead we were lead to consider fin-based swimming creatures. Kato and Furushima

(1996) had already proceeded down the path of paired fin swimming, drawing inspiration from the black bass to design rigid pectoral fins and incorporate them into a test-bed vehicle. He subsequently pursued low-speed maneuvering using rigid pectoral fins (Kato, 2000) and then went on to develop a passive flexible fin and an active pneumatic actuator pectoral fin (Kato et al., 2008). Barrett and Triantafyllo (1995) on the other hand had taken their inspiration from the undulating body and oscillating caudal fin of the tuna to design and build their flexible “Robotuna.” We looked for a fish which possessed the dynamic performance characteristics we needed and for which experimental measurements of swimming dynamics, including fin kinematics, already existed. Experimental observations of pectoral fin muscle activity, kinematics, and dynamics in coral reef wrasses (Westneat & Walker, 1997; Walker & Westneat, 1997) have shown that the body is essentially held rigid during straight-line motion, thus satisfying our rigid hull constraint. Very rapid (~10 body lengths per second) translational motions were observed (Walker & Westneat, 2000) to give comparable swimming performance to that seen in body-caudal fin swimmers of comparable size even though there was no contribution from body undulation or caudal fin oscillation in the wrasses. This solution offered the potential of fast forward swimming (or position-keeping in strong currents) while avoiding the complexity of a flexible hull. In addition, Walker and Westneat (1997) had observed high maneuverability by these swimmers in their complex reef habitats. These habitats are reasonable representations of our vehicle’s projected operating environment, hence we saw the possi-

bility of obtaining both high forward speed and excellent low-speed maneuvering and hovering performance as well.

The fish we selected to inspire our design was one of the coral reef pectoral fin swimmers, the bird wrasse (*Gomphosus varius*), shown in Figure 1.

FIGURE 1

Bird wrasse (*Gomphosus varius*).



Controlled Deformation Fin Technology Development

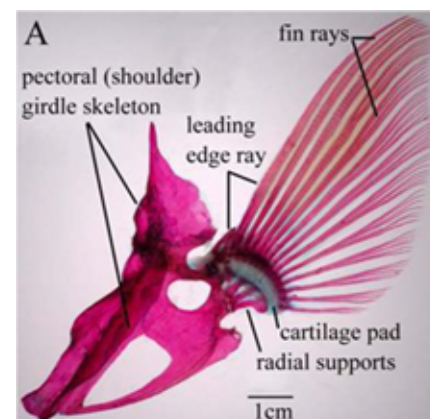
Living creatures, such as insects, birds, and pectoral fin swimmers, generate lift and thrust by executing large-amplitude wing/fin flapping, often with substantial shape deformation from root to tip and leading edge to trailing edge. The flow for these motions is three-dimensional and unsteady, and conventional steady-state aerodynamics is unable to correctly compute the corresponding time history of flapping-force generation. Comprehensive reports on the research carried out to study the fluid dynamics of flapping fins and wings (Rozhdestvensky & Ryzhov, 2003) and of biomimetic fins for underwater vehicles (Triantafyllo et al., 2004) exist, in addition to an extensive number of studies, too great to list here, on unsteady lift production by flapping insect wings. Three-dimensional unsteady computations are necessary to correctly predict the lift and thrust var-

iation throughout the flapping stroke cycle. Such computations, for creatures or vehicles with moving and deforming surfaces, provide the time-varying pressure distribution on all surfaces, which in turn can provide insights into how the flapping forces and maneuvering moments are being generated. This information can be coupled with computational visualization of the time-varying flow about the fish to analyze the origin of body and fin vorticity, its growth, and eventual shedding into the wake. This is the approach we developed for tuna caudal fin force production analysis (Ramamurti et al., 1996, 1999), subsequently validated against wrasse experimental data (Ramamurti et al., 2002), and which we also followed throughout our fin and vehicle development efforts described below.

There are 13 multiply bifurcating fin rays in the bird wrasse pectoral fin shown in Figure 2, each contributing to the fin curvature time-variation throughout the stroke cycle. For ease of design, manufacture, actuation, and control, it is ideal to have the fewest possible number of rays (which we refer to as ribs) and have each of them

FIGURE 2

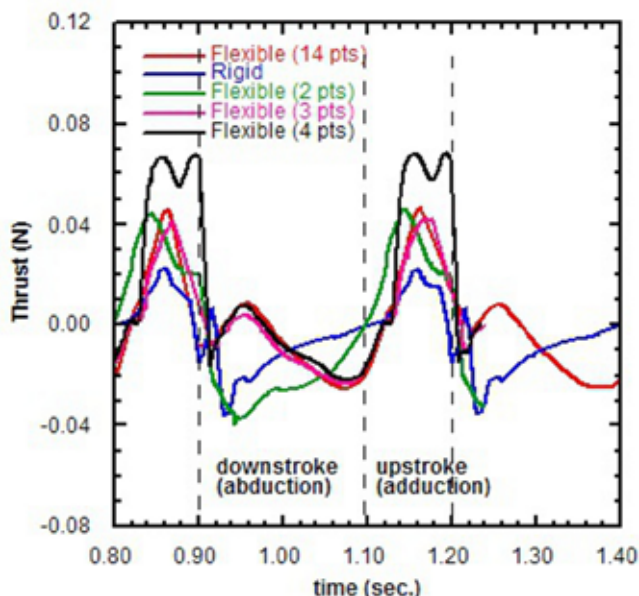
Bird wrasse fin structure (from Walker & Westneat, 1997).



be as simple in shape and structure as possible. But for more effective fin propulsion, it is ideal to maximize the number of ribs since more control points result in a smoother fit to desired fin curvature time-histories. Our computational investigations (Ramamurti et al., 2004) have shown that the loss of force magnitude over the stroke cycle is very small if we considerably reduce the number of ribs, as long as we maintain the ability to properly modify the surface curvature. The computations showed that when the fin was made rigid by specifying the motion with just the leading edge of the fin tip, the thrust produced during the upstroke was less than half of the peak thrust produced by the flexible fin computations. During the downstroke, the computations for the rigid and nearly rigid fin produced no positive thrust, while the partially and fully flexible cases produced substantial thrust. In the case of the rigid fin, there was also a substantial penalty in lift during the

FIGURE 3

Effect of fin flexibility on the time variation of thrust forces (from Ramamurti et al., 2004). (Color versions of figures available online at: <http://www.ingentaconnect.com/content/mts/mts/2011/00000045/00000004>.)



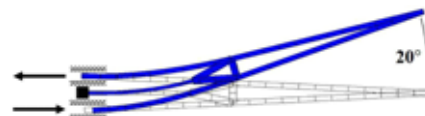
upstroke. An example from these computational investigations is shown below in Figure 3.

Assessment of these findings led us to reduce the number of ribs from 13 to 5. Five was selected since it enabled reduced fin complexity, thus substantially reducing fin size and weight, while maintaining the critically important flexural capability. Each of the five fin rays were individually designed and constructed from compliant ABS plastic material using a 3-D printer to achieve the desired tip deflection with an achievable linear actuation force applied to each individual rib at the root (Trease et al., 2003), as illustrated in Figure 4. The pushing and pulling of the ribs at the root of the fin is similar to how fish bend their ribs using muscle actuation.

The root section of the fin was selected to be of rectangular cross section with rounded leading edges and a tapered trailing edge in order to accommodate the actuators at the base of the ribs as shown in Figure 5a. A translu-

FIGURE 4

Representative rib cross-sectional geometry and bending analysis showing a 20° rib deflection.



cent silicone rubber membrane skin, optimized in thickness to approximately 0.5 mm via finite-element analysis (Palmisano et al., 2007), provided the continuous surface covering for the rays as shown in Figure 5b.

After several parametric 3-D unsteady computational fluid dynamics (CFD) studies had been carried out (Ramamurti & Sandberg, 2006), various fin parameters were chosen that optimized thrust performance, given the mechanical constraints of the fin. An example of these computations showing the variation of lift and thrust as a function of fin flexibility, stroke amplitude, and fin stroke bias is shown in Figure 6.

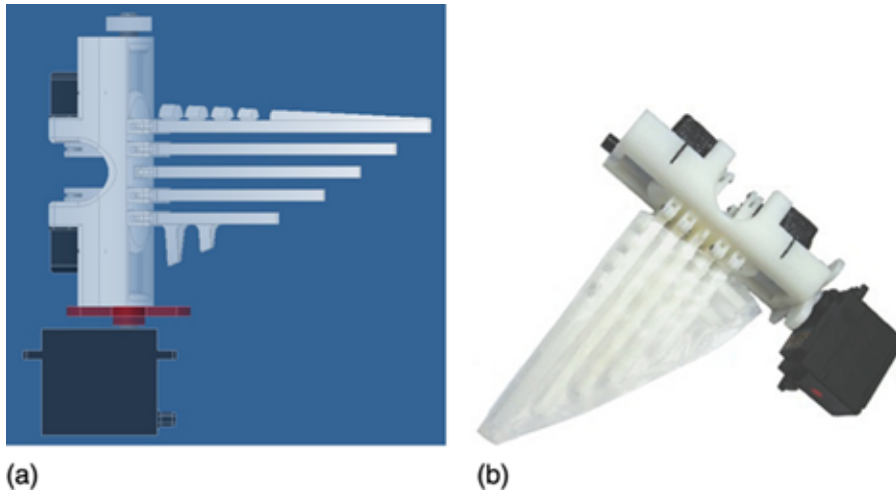
The angle of attack of the root section of the fin was chosen to be 20°, the amplitude of the oscillation to be 114°, the flapping frequency to be 1 Hz, and the rib spacing to be the minimum possible value of 1.2 cm dictated by the size of the actuators. These specific values, selected for maximizing fin force production, are for a solitary flapping and deforming fin. Incorporation of the fin into a vehicle design presents challenges to retain fin performance while maintaining vehicle simplicity.

Two-Fin Test-Bed Vehicle

A simple vehicle was designed and built to serve as a test-bed for evaluating the performance of all aspects of

FIGURE 5

Mechanical fin (a) CAD image without skin and (b) actual with skin.

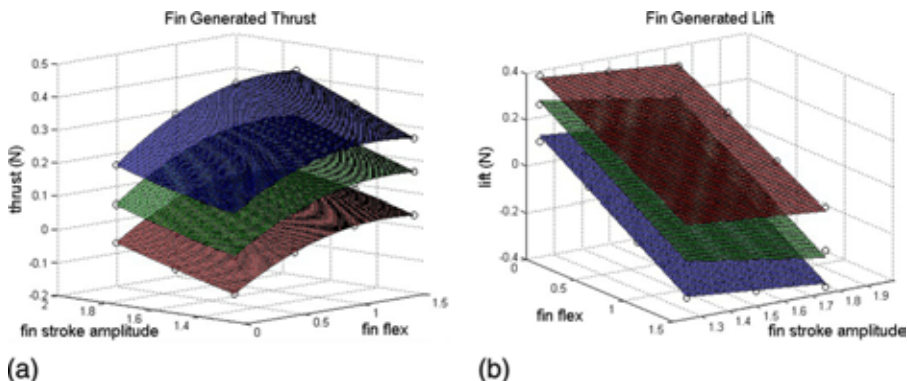


the controlled curvature fin technology, including its capability for vehicle propulsion, low-speed maneuvering, and hovering. It was, therefore, intentionally, a minimalist design that served to house the fins, actuators, and a battery. We described above how the parameters that govern the force production by the fin were chosen. However, due to mechanical constraints and a desire to easily manufacture a vehicle prototype, additional 3-D unsteady CFD studies of the flapping fins incorporated in the

test-bed vehicle led us to modify the fin-alone values. The angle of attack of the root section of the fin was chosen to be 0° , and the rib spacing was reduced to 0.8 cm. It is during construction tradeoffs of this type that one relies upon what has been learned from the studies of nature to meet operational performance goals while balancing that with the desire to create a vehicle that is producible at a reasonable cost. Fixing the fin root at a specific angle deviates from nature, but the construction simplicity and cost

FIGURE 6

Mean fin generated (a) thrust and (b) lift as functions of non-dimensionalized stroke amplitude and fin flex, or curvature. The surfaces indicate a bias in the fin stroke angle of 0° (red), 20° (green), and 40° (blue).



savings are so substantial that some performance penalty was accepted. The flapping stroke amplitude and frequency, as well as the phasing of the individual fin tip deflection time histories, were retained as controllable parameters, and we have performed CFD analyses of force production with this fin configuration (Ramamurti et al., 2010).

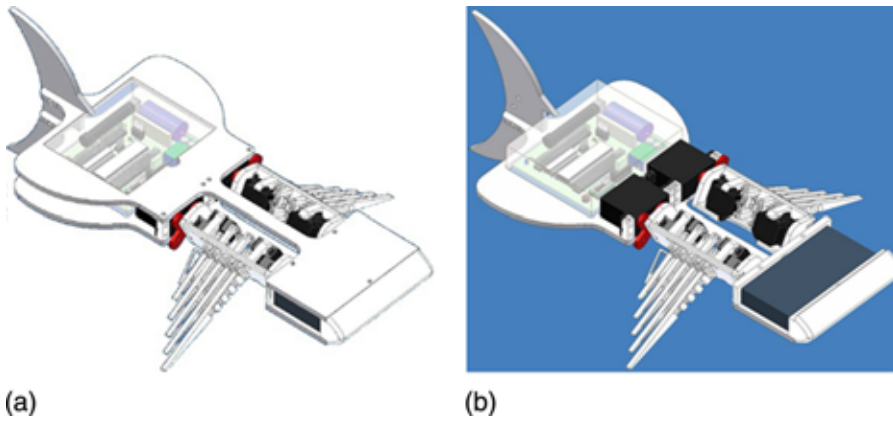
In keeping with the review nature of this paper, we are emphasizing *the process* carried out for our specific bio-inspired vehicle design. The details of the controlled curvature fin design, the linear actuator design and construction, the isolated fin construction and testing, the vehicle design, the vehicle construction, the experimental testing, and the validation of computations were previously reported (Palmisano et al., 2007, 2008; Sandberg & Ramamurti, 2008). The fin technology test-bed demonstration vehicle incorporated two actively controlled deformation fins. The two-fin vehicle is shown in Figure 7.

Four-Fin Test-Bed Vehicle

The test results for the two-fin vehicle demonstrated that the controlled deformation fin force production was capable of meeting our vehicle propulsion (position-keeping in a current) requirements (Geder et al., 2008). However, by design, this test-bed fin technology demonstration vehicle had restricted options for sensor payload and did not have the fore-aft force production capability needed for heave-pitch control. Hence, the design of a larger 41-cm long four-fin vehicle was initiated (Figure 8). The fore-aft symmetry of the four-fin design enables hover and higher precision positioning capabilities by decoupling vehicle pitch and heave control.

FIGURE 7

Two-fin technology test-bed demonstration vehicle: (a) exterior view and (b) interior view.



The current four-fin vehicle design shown here employs a water-tight cylinder for housing the power source and electronics with a flooded space in the nose and tail for buoyancy trimming and supplemental sensors. Hardware control and all computations are performed by a 16-MHz ATmega2560 microcontroller. Computations (Ramamurti et al., 2010) and experimental tests carried out to date (Geder et al., 2011) characterized how changes in fin stroke amplitude, frequency, bias angle, and curvature affect the thrust and lift forces for zero free stream flow speed. Further testing and computations are ongoing to fully characterize the fin forces and vehicle dynamics. However, current models have the necessary fidelity to accurately predict vehicle performance as outlined in the following sections.

Four-Fin Vehicle Control

With the vehicle state variables defined as in Figure 8, the vehicle dynamics can be written as,

$$M\dot{\mathbf{v}} + C(\mathbf{v})\mathbf{v} + D(\mathbf{v})\mathbf{v} + \mathbf{g}(\boldsymbol{\eta}) = \boldsymbol{\tau}, \quad (1)$$

where M is a matrix of rigid body mass and inertial terms, C is a matrix of centripetal and Coriolis terms, D is a matrix of hydrodynamic lift and drag terms, \mathbf{g} is a vector of hydrostatic terms, $\mathbf{v} = [u \ v \ w \ p \ q \ r]^T$, $\boldsymbol{\eta} = [x \ y \ z \ \phi \ \theta \ \psi]^T$ is the position and orientation vector in the earth-fixed frame where ϕ , θ , and ψ are roll, yaw, and pitch angles, and $\boldsymbol{\tau}$ is a vector of all forces and moments external to the rigid body. The portion of the vector, $\boldsymbol{\tau}$, that is effected by the fins is represented as,

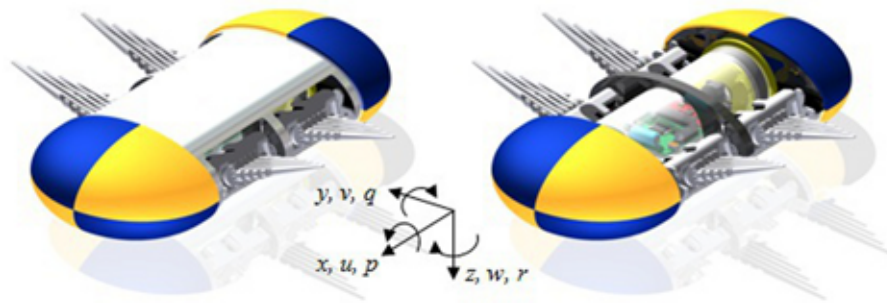
$$\boldsymbol{\tau}_{fins} = \begin{bmatrix} f_{T,LF} + f_{T,LB} + f_{T,RF} + f_{T,RB} \\ 0 \\ -f_{L,LF} - f_{L,LB} - f_{L,RF} - f_{L,RB} \\ -y_L(f_{L,LF} + f_{L,LB}) - y_R(f_{L,RF} + f_{L,RB}) \\ x_F(f_{L,LF} + f_{L,RF}) + x_B(f_{L,LB} + f_{L,RB}) \\ -y_L(f_{T,LF} + f_{T,LB}) - y_R(f_{T,RF} + f_{T,RB}) \end{bmatrix}, \quad (2)$$

where f_T is fin thrust and f_L is fin lift. Subscripts ‘LF’, ‘LB’, ‘RF’, and ‘RB’ identify the left front, left back, right front, and right back fins, respectively. The x -position of the center of pressure on the fins is denoted by x_F for the front fins and x_B for the back fins. The y -position of the center of pressure on the fins is denoted by y_L for the left fins and y_R for the right fins.

Mathematical models representing the dynamic performance of the fins have been developed to include the effects on force production of inflow velocities to the leading edge (or trailing edge for reverse motion) and to include the effects of fin interactions with each other, namely the effects of the trailing vortices off the front fins on the inflow to the back fins (Geder et al., 2011). Other fin dynamic representations modeled controllable parameters including fin curvature and stroke amplitude (Ramamurti et al., 2010). In the earlier 3-D unsteady CFD studies, these two key parameters were found to have a direct relationship with thrust generation—increasing stroke amplitude or fin curvature increased thrust (Ramamurti & Sandberg, 2006). However, since both stroke amplitude and flapping frequency are limited mechanically in the vehicle, optimal combinations of amplitude and frequency were experimentally found for high thrust and lift fin gaits. The best mix of these parameters for our vehicle was determined to be 100° for stroke amplitude and 1.8 Hz flapping frequency, which yielded not only high force output but also relatively low power consumption (Palmisano et al., 2007). These findings allowed us to fix stroke amplitude and frequency as constants and to focus on fin curvature as the primary thrust control parameter. Further, biasing the fin stroke up or down, as in Figure 9, affects fin lift

FIGURE 8

Four-fin technology test-bed vehicle, (a) exterior view, (b) interior view.



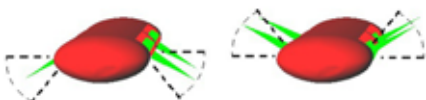
generation while maintaining constant thrust (Geder et al., 2008).

In previous work we evaluated the benefits of two vehicle control methods (Geder et al., 2008). The first method, called weighted gait combination, used combinations of thrust-generating and lift-generating fin gaits to produce vectored propulsive forces. The second method, called mean bulk angle bias (MBAB), used weighted forward-reverse gait control with stroke bias angle control. Between these two control methods, our results showed that MBAB better decoupled control over body-fixed thrust and lift forces and yielded better vehicle response characteristics in simulation. As such, the MBAB method is used to control the four-fin vehicle.

The vehicle controller commands changes to the fins to effect changes in the forces and moments imparted on the vehicle, as shown in equation 2. These fin commands are based on

FIGURE 9

Vehicle images showing all four fins with strokes (a) biased down to produce positive lift and (b) biased up to produce negative lift.



errors in the vehicle dynamic states, computed as the commanded values minus the computed values. States are computed onboard the vehicle using a suite of sensors (three axes of accelerometers, three axes of rate gyros, magnetic compass, and pressure sensor) and sensor fusion and filtering schemes (Geder et al., 2009). Errors in surge motion (x -axis translation) dictate commands for fin thrust changes to all fins. Errors in heave motion (z -axis translation) dictate commands for fin lift changes to all fins. Errors in roll motion (x -axis rotation) dictate commands for differential lift changes between left and right fins. Errors in

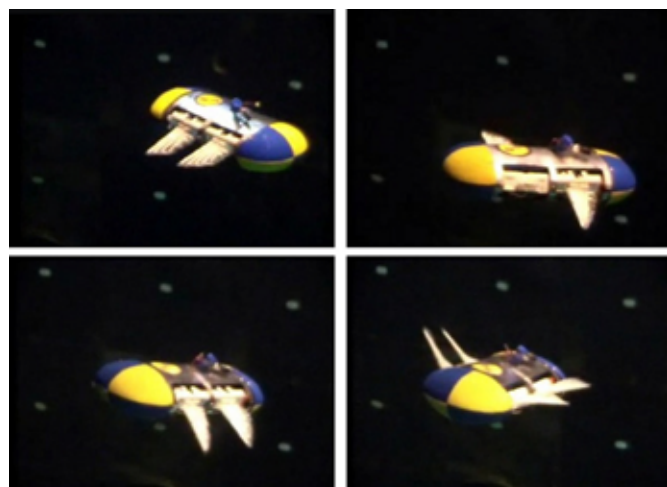
pitch motion (y -axis rotation) dictate commands for differential lift changes in forward and back fins. Errors in yaw motion (z -axis rotation) dictate commands for differential thrust changes in left and right fins. The vehicle has no direct control over sway motion (y -axis translation), and instead commands yaw motion changes to move in this direction. The direction of yaw motion depends on the sway error. The output of a proportional-integral-derivative (PID) controller for each vehicle state is used to determine forward and reverse fin gait percentage and bulk angle commands.

Four-Fin Vehicle Performance

Initial measurements of the dynamic performance of the four-fin vehicle have been conducted in two test facilities, one a $6 \times 2.5 \times 2$ foot water tank and the other a 50-foot diameter by 50-foot deep water tank (Figure 10). The experimental measurements have served to validate the vehicle dynamic model and to begin the assessment of vehicle performance.

FIGURE 10

Four-fin vehicle operating in a Naval Research Laboratory test facility.



An open loop test was conducted to characterize vehicle heading angle response and to compare model simulation performance with experimental performance (Geder et al., 2011). The right fins were set at full reverse kinematics, and the left fins were set to closely match the opposite thrust of the right fins. At $t = 11$ s, the gait weighting inputs were reversed. The simulated and experimental responses show very good agreement (Figure 11) with a maximum difference between the two responses at any given time of 5° . Both simulated and experimental results exhibit a $30^\circ/\text{s}$ maximum turning rate, 4 s time from zero to maximum speed, and braking angle of 35° —the amount of residual turning distance after fin kinematics are reversed.

After validating the four-fin vehicle dynamic model in yaw motion and implementing state feedback control, initial closed-loop experiments were done to test heading angle control (Geder et al., 2011). In Figure 12, a comparison of experimental and simu-

FIGURE 11

Comparison of experimental and simulated open-loop heading angle responses (from Geder et al., 2011).

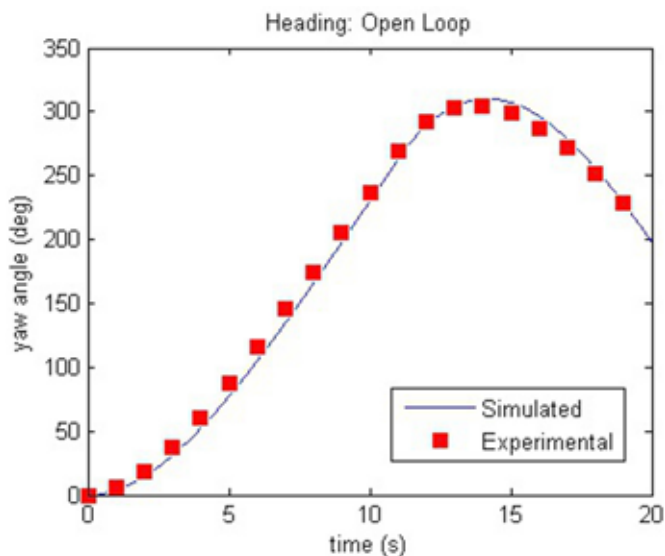
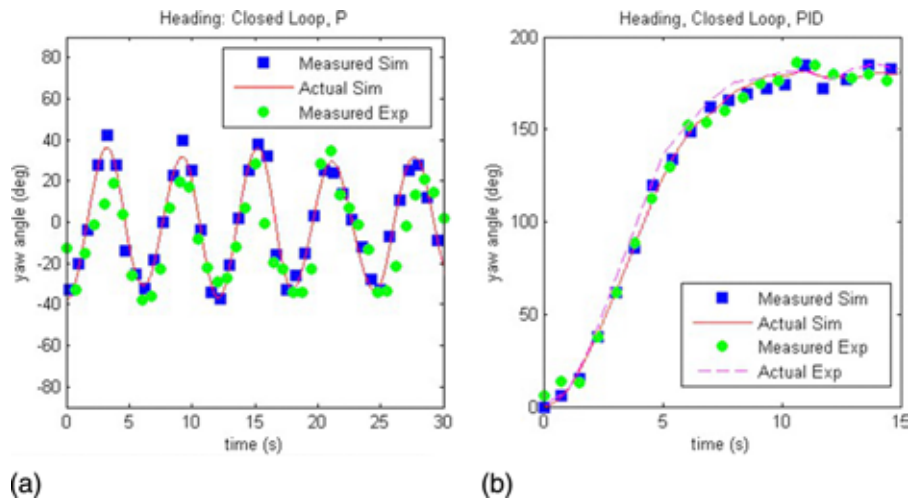


FIGURE 12

Comparison of experimental and simulated closed-loop heading angle responses with (a) proportional control and (b) PID control (from Geder et al., 2011). The solid curve represents the actual simulated heading response of the vehicle based on the modeled dynamics. The dashed curve represents the actual experimental heading response observed in vehicle testing. The square data represent the measured heading response of the vehicle based on the output of sensor models. The circle data represent the measured experimental vehicle heading from the output of on-board sensors.



lated results is given. For a simple proportional control algorithm (Figure 12a), we see the results match well with a $30\text{--}40^\circ$ amplitude and 6.5-s period. Dif-

ferences between measured experimental heading from onboard sensors and simulated heading can be attributed to the noise and sensitivity characteristics of the sensors (Geder et al., 2009). External magnetic disturbances in our test facility cause errors up to 10° in heading measurements, also factoring into the variation between experimental and simulated heading responses, as our calibration of the onboard compass was not perfect. Adding in a derivative gain to damp the heading response and a small integral gain to eliminate any steady-state error, we see the response to a 180° step command in heading in Figure 12b. With PID control over heading angle, the response is nearly critically damped with a rise time of 7 s. We also see close agreement between measured and actual angles, and again differences in the responses can be attributed to sensor noise and sensitivity, as well as compass calibration errors.

Conclusions

We have reviewed the history of our bioinspired vehicle design process. The process began by collaborating with biologists in order to understand the dynamics of flapping and deforming fins in pectoral fin swimmers. The detailed kinematics they measured in fish swimming experiments provided the time-varying fin surface curvature data necessary for computing the 3-D unsteady flow about the swimming fish. Examination of the computed flow variations about the flapping and deforming fins and the fish body provided insights into the relationship between the fin flows and the fin force time-histories throughout the stroke cycle. Parametric variations of key stroke parameters in 3-D unsteady flow computations yielded the sensitivity of the time-varying fin forces, which in turn provided the information needed to modify our fin design from that of the bird wrasse. It is during such computations that insights from nature can be blended with design constraints to yield a range of possible bio-inspired designs. A controlled curvature fin utilizing individually designed fin ribs, each actuated at the rib root by a linear actuator was built and tested. The successful fin tests were followed by the design and construction of a two-fin test-bed vehicle to demonstrate the mobility potential of the concept. Incorporation of the fins into a vehicle necessitated further compromises where we balanced biomimetic performance with produceability and cost. These test-bed vehicle tests were followed by the design and construction of a more capable four-fin vehicle, incorporating the same fins. A series of controllers were developed and built to enable assessment of vehicle propul-

sion and maneuvering performance as a function of the varying kinematics of each fin. Deforming fin force time histories, including fin-fin unsteady interactions, have been incorporated into the vehicle dynamic model used for controller development. The preliminary four-fin vehicle dynamic performance measurements indicate very good agreement with computed performance. These initial results are very encouraging and indicate that our efforts to emulate the position-keeping, low-speed maneuvering, and hovering performance of the bird wrasse into a producible and low cost vehicle are bearing fruit.

Lead Author:

Jason D. Geder
Laboratory for Computational
Physics and Fluid Dynamics
Naval Research Laboratory
Overlook Avenue, SW,
Washington, DC
Email: jgeder@lcp.nrl.navy.mil

References

- Alexander**, R.M. 1983. The history of fish biomechanics. In: *Fish Biomechanics*, eds. Webb, P.W., & Weihs, D., 1-35. New York: Praeger.
- Azuma**, A. 1992. *The Biokinetics of Flying and Swimming*. Tokyo: Springer-Verlag. 265 pp.
- Barrett**, D.S., & Triantafyllo, M.S. 1995. The design of a flexible hull undersea vehicle propelled by an oscillating foil. In: *Proc. 9th Int. Symp. on Unmanned Untethered Submersible Technology*. Durham, NH: Autonomous Undersea Systems Institute (AUSI).
- Bartol**, I.K., Gharib, M., Weihs, D., Webb, P.W., Hove, J.R., & Gordon, M.S. 2003. Hydrodynamic stability of swimming in ostraciid fishes: role of the carapace in the smooth trunkfish *Lactophrys triqueter* (Teleostei: Ostraciidae). *J Exp Biol.* 206: 725-44. doi: 10.1242/jeb.00137.
- Blake**, R.W. 1983. *Fish Locomotion*. Cambridge, UK: Cambridge University Press. 228 pp.
- Breder**, C.M. 1926. The locomotion of fishes. *Zoologica.* 4:159-297.
- Collar**, D., Wainwright, P., & Alfaro, M. 2008. Integrated diversification of locomotion and feeding in labrid fishes. *Biol Lett.* 4:84-6. doi: 10.1098/rsbl.2007.0509.
- Combes**, S., & Daniel, T. 2001. Shape, flapping, and flexion: wing and fin design for forward flight. *J Exp Biol.* 204:2073-85.
- Drucker**, E.G., & Lauder, G.V. 1999. Locomotor forces on a swimming fish: Three-dimensional vortex wake dynamics quantified using digital particle image velocimetry. *J Exp Biol.* 203:2393-412.
- Drucker**, E.G., & Lauder, G.V. 2002. Experimental hydrodynamics of fish locomotion: Functional insights from wake visualization. *Integr Comp Biol.* 42:243-57. doi: 10.1093/icb/42.2.243.
- Geder**, J.D., Palmisano, J., Ramamurti, R., Sandberg, W.C., & Ratna, B. 2008. Fuzzy logic PID-based control design and performance for pectoral fin-propelled unmanned underwater vehicle. In: *Proc. Int. Conf on Control, Automation and Systems*. Seoul, Korea: IEEE. doi: 10.1109/ICCAS.2008.4694526.
- Geder**, J.D., Ramamurti, R., Palmisano, J., Pruessner, M., Ratna, B., & Sandberg, W.C. 2009. Sensor data fusion and submerged test results of a pectoral fin propelled UUV. In: *Proc. 16th Intl Symp on Unmanned Untethered Submersible Technology*. Durham, NH: Autonomous Undersea Systems Institute (AUSI).
- Geder**, J.D., Ramamurti, R., Palmisano, J., Pruessner, M., Sandberg, W.C., & Ratna, B. 2011. Four-fin bio-inspired UUV: modeling

- and control solutions. ASME Intl Mech Eng Congress Exposition. IMECE. 2011-64005.
- Gharib, M., Pereira, F., Dabiri, D., Hove, J.R., & Modarress, D.** 2002. Quantitative flow visualization: Toward a comprehensive flow diagnostic tool. *Integr Comp Biol*. 42:964-70. doi: 10.1093/icb/42.5.964.
- Gibb, A.C., Jayne, B.C., & Lauder, G.V.** 1994. Kinematics of pectoral fin locomotion in the bluegill sunfish *Lepomis Macrochirus*. *J Exp Biol*. 189:133-61.
- Kato, N.** 2000. Control performance in the horizontal plane of a fish robot with mechanical pectoral fins. *IEEE J Oceanic Eng*. 25:125-9. doi: 10.1109/48.820744.
- Kato, N., Ando, Y., Tomokazu, A., Suzuki, H., Suzumori, K., Kanda, T., & Endo, S.** 2008. Elastic pectoral fin actuators for biomimetic underwater vehicles. In: *Bio-mechanisms of Swimming and Flying*, eds. Kato, N., Kamimura, S., 271-82. Tokyo: Springer.
- Kato, N., & Furushima, M.** 1996. Pectoral fin model for maneuver of underwater vehicles. In: *Proc. Symp. on Autonomous Underwater Vehicle Technology*. Monterrey, CA: IEEE. doi: 10.1109/AUV.1996.532400.
- Lindsey, C.C.** 1978. Form, function, and locomotory habits in fish. In: *Fish Physiology* Vol. II, eds. Hoar, W.S., & Randall, D.J., 1-100. New York: Academic Press.
- Palmisano, J., Geder, J.G., Ramamurti, R., Liu, K.J., Cohen, J.J., Mengesha, T., ... Ratna, B.** 2008. Design, development and testing of flapping fin with actively-controlled curvature for an unmanned underwater vehicle. In: *Bio-mechanisms of Swimming and Flying*, eds. Kato, N., & Kamimura, S., 283-94. Tokyo: Springer. doi: 10.1007/978-4-431-73380-5_23.
- Palmisano, J., Ramamurti, R., Liu, K.J., Cohen, J., Sandberg, W.C., & Ratna, B.** 2007. Design of a bio-mimetic controlled-curvature robotic pectoral fin. In: *Proc. IEEE Intl. Conf. on Robotics and Automation*. Rome, Italy: IEEE. doi: 10.1109/ROBOT.2007.363110.
- Ramamurti, R., Geder, J.D., Palmisano, J., Ratna, B., & Sandberg, W.C.** 2010. Computations of flapping flow propulsion for unmanned underwater vehicle design. *AIAA J*. 48(1):188-201. doi: 10.2514/1.43389.
- Ramamurti, R., Lohner, R., & Sandberg, W.C.** 1996. Computation of the unsteady flow past a tuna with caudal fin oscillation. In: *Advances in Fluid Mechanics*, eds. Rahman, M., & Brebbia, C., vol. 9, 169-78. Southampton, UK: Computational Mechanics Publishing.
- Ramamurti, R., Lohner, R., & Sandberg, W.C.** 1999. Computation of the 3-D unsteady flow past deforming geometries. *Int J Comput Fluid D*. 13:83-99. doi: 10.1080/10618569908940891.
- Ramamurti, R., & Sandberg, W.C.** 2006. Computational fluid dynamics study for optimization of a fin design. In: *Proc. 24th AIAA Applied Aerodynamics Conference*. AIAA. AIAA-2006-3658.
- Ramamurti, R., Sandberg, W.C., & Lohner, R.** 2004. The influence of fin rigidity and gusts on the force production in fish and insects: a computational study. In: *Proc. 42nd AIAA Aerospace Sciences Meeting and Exhibit*. Am Inst Aeronautics and Astronautics. AIAA-2004-0404.
- Ramamurti, R., Sandberg, W.C., Lohner, R., Walker, J.A., & Westneat, M.W.** 2002. Fluid dynamics of flapping aquatic flight in the bird wrasse: 3-D unsteady computations with fin deformation. *J Exp Biol*. 205:2997-3008.
- Rozhdestvensky, K.V., & Ryzhov, V.A.** 2003. Aerohydrodynamics of flapping-wing propulsors. *Prog Aerosp Sci*. 39:585-633. doi: 10.1016/S0376-0421(03)00077-0.
- Sandberg, W.C., & Ramamurti, R.** 2008. 3-D Unsteady computations of flapping flight in insects, fish, and unmanned vehicles. In: *Bio-mechanisms of Swimming and Flying*, eds. Kato, N., & Kamimura, S., 205-217. Tokyo: Springer. doi: 10.1007/978-4-431-73380-5_17.
- Sfakiotakis, M., Lane, D.M., & Davies, J.B.C.** 1999. Review of fish swimming modes for aquatic locomotion. *J Exp Biol*. 24:241-52.
- Trease, B.P., Liu, K.J., & Kota, S.** 2003. Biomimetic compliant system for actuator-driven aquatic propulsor: preliminary results. In: *ASME Intl. Mech. Eng. Congress and Exposition*. IMECE 2003-41446.
- Triantafyllo, M.S., Techet, A.H., & Hover, F.S.** 2004. Review of experimental work in biomimetic foils. *IEEE J Oceanic Eng*. 29:585-94. doi: 10.1109/JOE.2004.833216.
- Videler, J.J.** 1993. *Fish Swimming*. London, UK: Chapman and Hall. 260 pp.
- Wainwright, P., Bellwood, D., & Westneat, M.W.** 2002. Ecomorphology of locomotion in labrid fishes. *Environ Biol Fish*. 65:47-62. doi: 10.1023/A:1019671131001.
- Walker, J.A., & Westneat, M.W.** 1997. Labriform propulsion in fishes: Kinematics of flapping aquatic flight in the bird wrasse *Gomphosus varius* (Labridae). *J Exp Biol*. 200:1549-69.
- Walker, J.A., & Westneat, M.W.** 2000. Mechanical performance of aquatic rowing and flying. *P Roy Soc Lond B Bio*. 267: 1875-81. doi: 10.1098/rspb.2000.1224.
- Webb, P.W.** 1975. Hydrodynamics and energetics of fish propulsion. *Bull Fish Res Bd Can*. 190:1-158.
- Webb, P.W.** 1984. Form and function in fish swimming. *Sci Amer*. 251:58-68.
- Webb, P.W.** 2004. Maneuverability—General issues. *IEEE J Oceanic Eng*. 29:547-53. doi: 10.1109/JOE.2004.833220.
- Westneat, M.W., & Walker, J.A.** 1997. Motor patterns of underwater flight: an electromyographic study of the pectoral muscles in the bird wrasse, *Gomphosus varius*. *J Exp Biol*. 200:1881-93.